Comput Mech (2012) 50:805–819
DOI 10.1007/s00466-012-0768-9

ORIGINAL PAPER

A coupled PFEM–Eulerian approach for the solution of porous FSI problems

A. Larese · R. Rossi · E. Oñate · S. R. Idelsohn

Received: 4 July 2012 / Accepted: 17 July 2012 / Published online: 2 August 2012
© Springer-Verlag 2012

Abstract This paper aims to present a coupled solution strategy for the problem of seepage through a rockfill dam taking into account the free-surface flow within the solid as well as in its vicinity. A combination of a Lagrangian model for the structural behavior and an Eulerian approach for the fluid is used. The particle finite element method is adopted for the evaluation of the structural response, whereas an Eulerian fixed-mesh approach is employed for the fluid. The free surface is tracked by the use of a level set technique. The numerical results are validated with experiments on scale models rockfill dams.

Keywords PFEM · Level set · Lagrangian–Eulerian coupling · Seepage · Non-linear Darcy · Bingham plastics

1 Introduction

Many dams and dikes exhibit now a higher potential to experience overtopping during exceptional flood events. Climate change induced by global warming is, for instance, one of the main causes that might lead to more devastating flooding.

While in a concrete dam an overflow is not likely to affect the integrity of the structure, in an embankment dam it usually compromises the dam body [11]. If a dam or dike fails, loss of life and economic damage are direct consequences of such event. That is the reason why there is an increasing interest on the study of rockfill dams during extreme phenomena.

The analysis of the possible consequences of an accidental overspill is still impossible or very imprecise and the necessary economical measures for solving the problem are therefore inefficient. An appropriate computational method would help reducing the cost of the investments needed in dam safety and emergency plans for rockfill dams.

The possibility of studying the behavior of water throughout and over the dam in case of a sudden change of the upstream conditions and its effect on the rockfill is currently limited by the absence of a suitable numerical tool. This should simulate the sudden dynamic change in the seepage and flow condition and predict the subsequent onset and evolution of breaching in the rockfill slope. The current work aims to contribute to this field, creating and validating a new computational method of general applicability for simulating, with a unique formulation, the flow throughout and over the dam while failure occurs together with the dam structural response.

Traditionally the coupled problem of soils or rock and water is faced using a multiphase material whose behavior is governed by the coupling between the different phases: soil, water and air. The first mathematical models describing the coupling of the solid and fluid phases were developed by Biot [2]. Nevertheless his work was only suitable for linear elastic materials and its extension to non-linear problems with large deformations was carried on only several years later by Zienkiewicz and Shiomi [41]. Its should be mentioned that important steps forward in this field have been made recently by Lewis and Schrefler [14], Coussy [21] and De Boer [3]. These well established approaches in geomechanics were not considered as an alternative in the present work for the following reasons:

A. Larese · R. Rossi · E. Oñate · S. R. Idelsohn (✉)
Centre Internacional de Mètodes Numèrics en Enginyeria (CIMNE), Barcelona, Spain
e-mail: sergio@cimne.upc.edu

A. Larese · R. Rossi · E. Oñate
UPC, BarcelonaTech, Campus Norte, 08034 Barcelona, Spain

S. R. Idelsohn
Intitució Catalana de Recerca i Estudis Avançats (ICREA), Barcelona, Spain

– The possibility of accurately following the transient regime of the water flow throughout and over the rockfill is a key point of the model. The coupling of these two phenomena would be very challenging using the traditional models, needing the transferring of interface conditions between the free surface problem and the seepage one. On the contrary, in the present work this is automatically taken into account with a unique fluid formulation.
– Considering the saturation level and the interaction between air and water in the partially saturated pores, becomes useless. In fact, according to experimental evidence the problem of interest can be considered fully drained, being the pores interconnected.
– Due to the time scale of the exceptional flooding, which can be of the order of minutes or maximum hours, the dam rockfill material can be considered as rigid (avoiding any elastic response in the unyielded region) and its compressibility can be neglected.
– The capability of tracking the material yield surface is not needed.

Both fluid and structure balance equations have to be derived from the imposition of the global equilibrium. For that purpose in the following sections the "monolithic" global problem is used to obtain the balance equations for the structure. Once the fluid and the structural problems are defined, the coupling strategy is presented. Different kinematic frameworks are used for the fluid and the structural problem: an Eulerian and a Lagrangian approach respectively. This choice leads to the definition of a staggered loosely-coupled scheme. A key point of the coupled tool is the possibility of transferring information between the moving and the fixed mesh. For such purpose a mapping between non matching meshes has been developed.

All the algorithms presented in this paper are implemented inside Kratos multiphysics [9] available on-line at http://kratos.cimne.upc.edu.

2 Mathematical model

Let us consider the balance equations of the global coupled problem in a domain Ω for time $t \in (0, T)$ which can be written as follows

$$\begin{aligned} &\rho_s \partial_t \mathbf{u}_s + \rho_s \mathbf{a}_s \cdot \nabla^s \mathbf{u}_s + \nabla p'_s \\ &\quad - 2\nabla \cdot \overline{\mu} \nabla^s \mathbf{u}_s - \rho_s \mathbf{b}_s + \rho_f \partial_t \mathbf{u}_f + \rho_f \mathbf{a}_f \cdot \nabla \mathbf{u}_f \\ &\quad + \nabla p_f - 2\nabla \cdot \mu_f \nabla^s \mathbf{u_f} - \rho_f n \mathbf{b}_f = \mathbf{0}; \\ &n\rho_f \nabla \cdot \mathbf{u}_f + \rho_s \nabla \cdot \mathbf{u}_s = 0; \end{aligned} \tag{1}$$

where the sub indexes s and f indicates the structural and the fluid variables respectively. The degrees of freedom (DOFs) of the problem are $\mathbf{u}_s$ and p'_s, i.e. the structural velocity and the effective pressure respectively, p_f, the fluid pressure and $\mathbf{u}_f$, the so called Darcy velocity. The latter is the fluid velocity averaged on the total areal. This velocity is related to the fluid velocity averaged on the empty area ($\overline{\mathbf{u}}_f$), by the Dupuit-Forchheimer equation [19] $\mathbf{u}_f = n\overline{\mathbf{u}}_f$ where n is the porosity. $\mathbf{a}_s$ and $\mathbf{a}_f$ are the structural and fluid convective velocity. In the problem of interest we shall take $\mathbf{a}_f = \overline{\mathbf{u}}_f$ in an Eulerian framework and $\mathbf{a}_s = \mathbf{0}$ since the structural problem will be treated using a Lagrangian technique. $\overline{\mu}$ and μ_f are the structural apparent viscosity (that will be discussed later on) and the fluid dynamic viscosity respectively.

The assumption of incompressibility is made for the global problem as well as for the fluid and structural problems.

The fluid and structural density are related by the definition of global density ρ. This can be either a dry density $\rho_s = (1-n)\overline{\rho_s}$ if the node is not immersed in water, or a nodal saturated density ρ_{sat}

$$\rho := \rho_{sat} = n\rho_f + (1-n)\overline{\rho}_s + = n\rho_f + \rho_s. \tag{2}$$

Finally $\mathbf{b}_f$ and $\mathbf{b}_s$ are the fluid and structural external force vectors.

2.1 Fluid model

The classical approaches of fluid flow in porous media are not applicable for the analysis of water motion within the rockfill of a dam. Traditionally water is considered in slow motion or as a stationary load [40]. On the contrary we are interested in the possibility of following the rapid transition of the water level within a rockfill slope as well as in its surroundings for identifying the beginning of the failure mechanism.

On the other hand, the typical problem of evaluating the saturation level of the pores loses its importance in the case studied due to the large dimension of the granular material. Under these circumstances, in fact, the pores can be considered always interconnected and the problem fully drained [38]. It should be pointed out that a key point for the complete fluid simulation of the hydrodynamic effect of an overtopping is the capability of the code to simulate at once, not only the seepage, but also the fluid flow upstream, downstream and over the rockfill. For that purpose the balance equations are derived considering the flow inside a generic porous material. This way the equations automatically reduce to the classical Navier-Stokes equations when porosity is equal to one, that is, when no porous medium is present.

A similar approach has been used by Nithiarasu and coworkers [20] to study the natural and forced convective flux in a cavity filled by a variable porosity medium.

The balance equation for the fluid problem are obtained imposing the conservation of mass and linear momentum in within a fixed control volume (the details of the derivation can be found in [12])

$$\rho_f \partial_t \mathbf{u}_f + \rho_f \overline{\mathbf{u}}_f \cdot \nabla \mathbf{u}_f + n \nabla p_f - 2\nabla \cdot \mu_f \nabla^s \mathbf{u}_f - \rho_f \mathbf{b}_f n + n\mathbf{D} = \mathbf{0}; \tag{3}$$

$$\nabla \cdot \mathbf{u}_f = 0; \tag{4}$$

In Eq. 3, $\mathbf{D}$ is the matricial form of the resistance law which is known as the Darcy term. It represents the dissipative effects due to the interaction between the solid and the fluid part. The resistance law should be chosen among the possible quadratic or exponential forms proposed in the literature [38]. In fact this cannot be taken in its linear form (Darcy's law) due to the characteristics of the problem that exceed the Darcy's law range of validity [34].

In this work the Ergun correlation has been chosen. The main purpose of this model is to treat with a unified formulation the free surface flow in presence or absence of a porous rockfill material. Between the existing options, this model was chosen since the D term automatically goes to zero when $n \to 1$ (open air).

Calling E_1 and E_2 the Ergun coefficients, the resistance law is

$$\mathbf{D} = E_1 \mathbf{u}_f + E_2 \mathbf{u}_f^2 = \frac{\mu_f}{k}\mathbf{u}_f + \frac{1.75}{\sqrt{150}}\frac{\rho_f}{\sqrt{k}}\frac{|\mathbf{u}_f|}{n^{3/2}}\mathbf{u}_f. \tag{5}$$

where k is the permeability defined as

$$k := \frac{n^3 D_{50}^2}{150(1-n)^2}. \tag{6}$$

where D_{50} is an equivalent diameter of the porous material[1] and

$$E_1 := 150 \cdot \frac{(1-n)^2}{n^3} \cdot \frac{\mu}{D_{50}^2}; \tag{7}$$

and

$$E_2 := 1.75 \cdot \frac{(1-n)}{n^3} \cdot \frac{\rho_f}{D_{50}}; \tag{8}$$

2.2 Structural model

The simulation of the structural response of a slope made of granular material has been treated using a continuous approach despite the intrinsic incoherent nature of the rockfill. This is an acceptable choice under the assumption that the rockfill size is small with respect to the overall size of the structure.

It should be mentioned that in recent years, the important advances in computer performance and in parallel computing have allowed the simulation of large domains taking into account the behavior of every single particle of a granular slope. The family of the so called discrete (or distinct) element methods (DEM) is reaching widespread popularity in the computational mechanics community. The basic idea is that every particle is a discrete element interacting with the others considering its mechanical and material properties [29,39].

The adoption of a continuous approach implies the choice of a suitable constitutive law. Many plastic or rigid-plastic constitutive models are commonly used in geomechanics to describe the structural response of an incoherent non-cohesive material [40]. It is usually accepted that a rockfill slope has the capability to support a certain amount of shear stress with almost no elastic strains before starting large deformation. When the yield stress is reached the material starts to *flow* until arriving at a stable configuration. It should be remarked that the behavior of the yielded material is more similar to the flowing of a fluid than to the process of deformation of a solid. In the literature there exists a wide category of fluids which exhibits a rigid behavior until reaching a yield threshold. They are part of the family of the so called non-Newtonian fluids.

These aspects, together with the natural way of managing large deformations in fluids, lead us to concentrate on variable viscosity models for the calculation of the structural response instead of any other plastic or damage models. Consequently, a non-Newtonian constitutive law was adopted for the rockfill body.

The Bingham bilinear behavior might induce numerical difficulties, hence smooth laws are usually preferred. Some authors [15] attempted to simulate the so called bi-viscosity model but their predictions lead to inconsistencies. Consequently, in the present work the regularized model proposed by Papanastasiou [27] is chosen as a starting point for the development.

Following the ideas presented in [27], the $3D$ Bingham regularized relation[2] is

$$\boldsymbol{\tau}_s = 2\left[\mu_s + \frac{\tau_0}{\dot{\gamma}}\left(1 - e^{-m\dot{\gamma}}\right)\right]\boldsymbol{\varepsilon}_s(\mathbf{u}_s), \tag{9}$$

where m is a regularization parameter that controls the approximation to the bilinear model as shown in Fig. 1. The apparent viscosity is therefore defined as

$$\tilde{\mu}(\dot{\gamma}) = \mu_s + \frac{\tau_0}{\dot{\gamma}}\left(1 - e^{-m\dot{\gamma}}\right), \tag{10}$$

[1] D_{50} is the diameter of the sieve at which the 50 % of the material passed.

[2] In $3D$ the *equivalent strain rate* $\dot{\gamma}$ and *yield stress* τ_0 are defined as the second invariants of the rate of strain tensor ($\boldsymbol{\varepsilon}$) and of the deviatoric part of the stress tensor ($\boldsymbol{\tau}$), respectively.

$$\dot{\gamma} = \left(\frac{1}{2}\boldsymbol{\varepsilon}_s : \boldsymbol{\varepsilon}_s\right)^{\frac{1}{2}} \qquad \tau_0 = \left(\frac{1}{2}\boldsymbol{\tau}_s : \boldsymbol{\tau}_s\right)^{\frac{1}{2}}$$

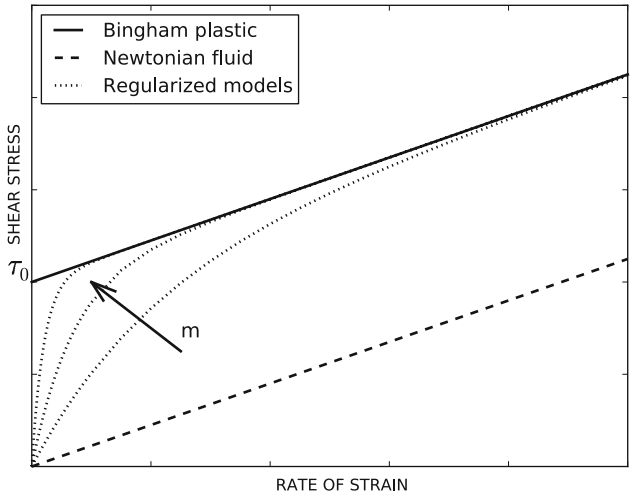

Fig. 1 Newtonian and Bingham fluid compared with the regularized model for increasing values of the m parameter

Referring to Eq. 10, the problems connected with the singular point of the bi-linear model are avoided here. In fact, in the un-yielded zone the shear strain rate $\tilde{\mu} = \mu + \tau_0\, m$ as $\dot{\gamma} \to 0$.

The Bingham model was originally conceived for materials with a fixed yield stress.

For granular materials, the definition of the yield stress depends on:

- The characteristics of the rockfill (its internal friction angle).
- The effective stress.

The model proposed in the present work has its origin in a classical Bingham constitutive relation, but using a pressure sensitive yield stress τ_0 defined using a Mohr–Coulomb failure criteria without cohesion.

$$\tau_0 = p'_s\, tg(\phi), \tag{11}$$

where p'_s is the effective pressure and ϕ is the internal friction angle. Equation 9 in $3D$ becomes

$$\boldsymbol{\tau}_s = 2\left[\mu_s + \frac{p'_s\, tg(\phi)}{\dot{\gamma}}\left(1 - e^{-m\dot{\gamma}}\right)\right]\boldsymbol{\varepsilon}_s(\mathbf{u}_s), \tag{12}$$

and the resulting apparent viscosity is therefore

$$\tilde{\mu}(\dot{\gamma}) = \mu_s + \frac{p'_s\, tg(\phi)}{\dot{\gamma}}\left(1 - e^{-m\dot{\gamma}}\right), \tag{13}$$

The idea of a pressure dependent yield stress has already been exploited for instance in [28], where a frictional fluid rehological model is used for the simulation of land slides.

The structural boundary value problem can therefore be derived subtracting 3 and 4 from 1. Let us consider a structural domain Ω_s and a time instance $t \in (0, T)$ the structural problem becomes

$$\begin{aligned} &\rho_s \partial_t \mathbf{u}_s + \rho_s \mathbf{a}_s \cdot \nabla^s \mathbf{u}_s + \nabla p'_s \\ &\quad - 2\nabla \cdot \tilde{\mu}_s \nabla \mathbf{u}_s - \rho_s \mathbf{b}_s + (1-n)\nabla p_f - \mathbf{D} = \mathbf{0} \\ &\nabla \cdot \mathbf{u}_s = 0, \end{aligned} \tag{14}$$

The problem is fully defined with the following boundary and initial condition:

$$\begin{aligned} &\mathbf{u}_s(\mathbf{x}, 0) = \mathbf{u}_{s\,0}(\mathbf{x}) && \text{in } \Omega_s, \\ &\mathbf{u}_s(\mathbf{x}, t) = \mathbf{g}_s(\mathbf{x}, t) && \text{on } \partial\Omega_{s\,D},\ t \in (0, T), \\ &\mathbf{n} \cdot \boldsymbol{\sigma}_s(\mathbf{x}, t) = \mathbf{t}_s(\mathbf{x}, t) && \text{on } \partial\Omega_{s\,N},\ t \in (0, T), \end{aligned} \tag{15}$$

where $\partial\Omega_{s\,D}$ and $\partial\Omega_{s\,N} = \Gamma_s$ are the Dirichlet and the Neumann boundaries respectively.

Remark 1 The D term in the coupled problem should take a form slightly different than Eq. 5

$$\mathbf{D} = \frac{n\,\mu_f}{k}(\mathbf{u}_f - \mathbf{u}_s) + \frac{1.75}{\sqrt{150}}\frac{\rho_f n}{\sqrt{k}}\frac{|\mathbf{u}_f - \mathbf{u}_s|}{n^{3/2}}(\mathbf{u}_f - \mathbf{u}_s). \tag{16}$$

where the relative velocity should be used. In practice, for the problem of interest the structural velocity is small with respect to the fluid one. Its effect is hence considered negligible and it is not taken into account. This is not the case if the same strategy is used in the calculation of, for example, a landslide into a reservoir or any other problem in which the structural velocity is comparable or even larger than the fluid one.

3 Numerical approach

The fluid and the structural problems presented in the previous section are treated in two different kinematical frameworks: the fluid problem is solved using an Eulerian fixed grid approach whereas for the structural one, a Lagrangian approach is preferred. This choice is the consequence of the following considerations:

The structure suffers large deformation and shape changes. For this purpose a Lagrangian approach results a natural choice. The particle finite element method (PFEM), a Lagrangian technique with remeshing is the adopted approach. On the other hand the fluid problem might be also treated with a Lagrangian approach, but the need of a frequent (and not parallel) remeshing would have considerably slowed the calculation down. We therefore prefer to reduce the fluid computational effort treating this part with a fixed mesh approach and a level set technique to track the evolution of the free surface. An edge-based approach is chosen since it is considered a more competitive choice than a traditional element based one [12] due to its simple parallelization [30,33].

3.1 Fluid numerical model

The fluid problem to be solved in a domain Ω for a time instance $t \in (0, T)$ is given by Eqs. 3 and 4 with the following boundary and initial conditions:

$$\begin{aligned} &\mathbf{u}_f(\mathbf{x}, 0) = \mathbf{u}_{f0}(\mathbf{x}) \qquad \text{in } \Omega; \\ &\mathbf{u}_f(\mathbf{x}, t) = \mathbf{g}_f(\mathbf{x}, t) \qquad \text{on } \partial\Omega_D,\ t \in (0, T); \\ &\mathbf{n} \cdot \boldsymbol{\sigma}_f(\mathbf{x}, t) = \mathbf{t}_f(\mathbf{x}, t) \text{ on } \partial\Omega_N,\ t \in (0, T); \end{aligned} \tag{17}$$

where $\partial\Omega_D$ and $\partial\Omega_N = \Gamma$ are the Dirichlet and the Neumann boundaries respectively. The weak form of Eqs. 3 and 4 is derived next using a Galerkin formulation. A mixed finite element method is used.

The weak form of Eqs. 3 and 4 integrating by part the viscous term is

$$\begin{aligned} &\int_\Omega \mathbf{w}_f \rho_f \partial_t \mathbf{u}_f d\Omega + \int_\Omega \mathbf{w}_f \rho_f \overline{\mathbf{u}}_f \cdot \nabla \mathbf{u}_f d\Omega \\ &+ \int_\Omega \mathbf{w}_f n \nabla p_f d\Omega + 2 \int_\Omega \nabla \mathbf{w}_f : \mu_f \nabla^s \mathbf{u}_f d\Omega \\ &+ \int_\Omega \mathbf{w}_f (E_1 \mathbf{u} + E_2 |\mathbf{u}_f| \mathbf{u}_f) d\Omega \\ &- \int_\Omega \mathbf{w}_f \rho_f n \mathbf{b}_f d\Omega - \int_{\partial\Omega_N} \mathbf{w}_f \cdot \mathbf{t}_f d\Gamma = \mathbf{0} \quad \forall \mathbf{w}_f \in \mathcal{V}; \\ &\int_\Omega q_f \nabla \cdot \mathbf{u}_f = 0 \quad \forall q_f \in \mathcal{Q}; \end{aligned} \tag{18}$$

where, for a fixed $t \in (0, T)$, $\mathbf{u}_f$ is assumed to belong to the velocity space $\mathcal{V} \in \mathbf{H}^1(\Omega)$, and p_f belongs to the pressure space $\mathcal{Q} \in \mathbf{H}^1(\Omega)$.$\mathbf{w}_f$ and q_f are velocity and pressure weighting functions belonging to the velocity and the pressure spaces respectively.

$\mathbf{H}^1$ continuity is required since the gradient of pressure term is not integrated by parts, as explained in [30] where a similar formulation is presented for a free surface incompressible fluid solver.

Let $\mathcal{V}_h$ be a finite element space to approximate $\mathcal{V}$, and $\mathcal{Q}_h$ a finite element approximation to $\mathcal{Q}$. The problem is now finding $\mathbf{u}_{fh} \in \mathcal{V}_h$ and $p_{fh} \in \mathcal{Q}_h$ such that

$$\begin{aligned} &\int_\Omega \mathbf{w}_{fh} \rho_f \partial_t \mathbf{u}_{fh} d\Omega + \int_\Omega \mathbf{w}_{fh} \rho_f \overline{\mathbf{u}}_{fh} \cdot \nabla \mathbf{u}_{fh} d\Omega \\ &+ \int_\Omega \mathbf{w}_{fh} n \nabla p_{fh} d\Omega + 2 \int_\Omega \nabla \mathbf{w}_{fh} : \mu_f \nabla^s \mathbf{u}_{fh} d\Omega \\ &+ \int_\Omega \mathbf{w}_{fh} (E_1 \mathbf{u}_{fh} + E_2 |\mathbf{u}_{fh}| \mathbf{u}_{fh}) d\Omega \\ &- \int_\Omega \mathbf{w}_{fh} \rho_f n \mathbf{b}_{fh} d\Omega - \int_{\partial\Omega_N} \mathbf{w}_{fh} \cdot \mathbf{t}_{fh} d\Gamma = \mathbf{0} \\ &\forall \mathbf{w}_{fh} \in \mathcal{V}_h; \\ &\int_\Omega q_{fh} \nabla \cdot \mathbf{u}_{fh} d\Omega = 0 \\ &\forall q_{fh} \in \mathcal{Q}_h; \end{aligned} \tag{19}$$

3.1.1 Edge-based approach

An edge-based approach is used in order to optimize the calculation of the fluid evolution. The idea is to express all the integral operators of the classical Galerkin discretization in terms of the neighboring contributions accessing each node only once and taking advance of the *Compressed Sparse Row* (*CSR*) matrix storing format and to pre-integrate all the necessary terms at the beginning of the calculation.

Since symmetry is not exploited in the present implementation, the parallelization of an edge-base code is straight forward [18]. Two nested loops are performed, the main loop (which is the one to parallelize) is made over the mesh node i, and the inner one is made over node j surrounding node i (the edges connected to node i).

Full details on the implementation of the operators are provided in [33] and [18].

3.1.2 Stabilized formulation

Since only simplicial P1/P1 elements are used in this work, a suitable stabilization technique is necessary to overcome pressure and convective instabilities. The *Orthogonal Subgrid Scale* OSS method introduced by Codina [5] is used. In this case the space for the sub-grid scale is taken orthogonal to the finite element one.

Following strictly the operations outlined in [7,33], the problem already presented in Eq. 19, with the insertion of the convection and incompressibility stabilization terms, is: find $(\mathbf{u}_{fh}, p_{fh}, \boldsymbol{\pi}_h, \boldsymbol{\xi}_h)$ in $\mathcal{V}_h \times \mathcal{Q}_h \times \mathcal{V}_h \times \mathcal{V}_h$ such that

$$\begin{aligned} &\int_\Omega \mathbf{w}_{fh} \partial_t \mathbf{u}_{fh} d\Omega + \int_\Omega \mathbf{w}_{fh} \overline{\mathbf{u}}_{fh} \cdot \nabla \mathbf{u}_{fh} d\Omega \\ &+ \int_\Omega \mathbf{w}_{fh} n \nabla p_{fh} d\Omega + 2 \int_\Omega \nabla \mathbf{w}_{fh} : \nu_f \nabla \mathbf{u}_{fh} d\Omega \\ &+ \int_\Omega \mathbf{w}_{fh} (\overline{E}_1 \mathbf{u}_{fh} + \overline{E}_2 |\mathbf{u}_{fh}| \mathbf{u}_{fh}) d\Omega - \int_\Omega \mathbf{w}_{fh} n \mathbf{b}_f d\Omega \\ &- \int_\Omega \tau (\overline{\mathbf{u}}_{fh} \cdot \nabla \mathbf{w}_{fh}) \mathcal{P}_h^\perp (\overline{\mathbf{u}}_{fh} \cdot \nabla \mathbf{u}_{fh} + \overline{E}_2 |\mathbf{u}_{fh}| \mathbf{u}_{fh}) d\Omega \\ &= \mathbf{0} \end{aligned}$$

$$\forall \mathbf{w}_{fh} \in \mathcal{V}_h;$$

$$\int_\Omega q_{fh} \nabla \cdot \mathbf{u}_{fh} d\Omega + \int_\Omega \tau \nabla q_{fh} \mathcal{P}_h{}^{\perp}(n \nabla p_{fh}) d\Omega = 0$$

$$\forall q_{fh} \in \mathcal{Q}_h; \tag{20}$$

where $\mathcal{P}_h{}^{\perp}$ is the space of *orthogonal projections* $\mathcal{P}_h{}^{\perp} = \mathcal{I} - \mathcal{P}_h$ and $\mathcal{P}_h$ is the L_2—*projection* onto $\mathcal{V}_h$. That is

$$\mathcal{P}_h{}^{\perp}(\overline{\mathbf{u}}_{fh} \cdot \nabla \mathbf{u}_{fh} + \overline{E}_2 |\mathbf{u}_{fh}| \mathbf{u}_{fh}) \tag{21a}$$

$$= \overline{\mathbf{u}}_{fh} \cdot \nabla \mathbf{u}_{fh} + \overline{E}_2 |\mathbf{u}_{fh}| \mathbf{u}_{fh} - \boldsymbol{\pi}_h;$$

$$\mathcal{P}_h{}^{\perp}(\nabla p_{fh}) = n \nabla p_{fh} - \boldsymbol{\xi}_h; \tag{21b}$$

with $\boldsymbol{\pi}_h$ and $\boldsymbol{\xi}_h$ defined as

$$\int_\Omega \mathbf{w}_{fh} \boldsymbol{\pi}_h d\Omega$$

$$= \int_\Omega \mathbf{w}_{fh} (\overline{\mathbf{u}}_{fh} \cdot \nabla \mathbf{u}_{fh} + \overline{E}_2 |\mathbf{u}_{fh}| \mathbf{u}_{fh}) d\Omega; \tag{22a}$$

$$\forall \mathbf{w}_{fh} \in \mathcal{V}_h$$

$$\int_\Omega \mathbf{w}_{fh} \boldsymbol{\xi}_h d\Omega = \int_\Omega \mathbf{w}_{fh} n \nabla p_{fh} d\Omega; \quad \forall \mathbf{w}_{fh} \in \mathcal{V}_h \tag{22b}$$

The additional unknowns $\boldsymbol{\xi}$ and $\boldsymbol{\pi}$ can be easily expressed in function of velocity and pressure through this equations.

Following the analysis of Codina [6], and considering the additional presence of the Darcy term, τ is defined as

$$\tau_i = \left(\frac{\alpha}{\Delta t} + \frac{4\nu_{fi}}{h_i^2} + \frac{2|\overline{\mathbf{u}}_{fi}|}{h_i} + (\overline{E}_1 + \overline{E}_2 |\mathbf{u_{fi}}|) \right)^{-1} \tag{23}$$

where h_i is the mesh size taken equal to the minimum edge length (l_{ij}) of the edges ij surrounding node i. α is a parameter that controls the importance of the dynamic term in the stabilization ($\alpha \in [0, 1]$). In the case of pressure stabilization we take $\alpha = 1$, whereas for the convective term, α it is taken equal to 0.01 therefore decreasing the importance to 1 %. Finally $\overline{E}_1$ and $\overline{E}_2$ are the Ergun's coefficients defined in 7 and 8 respectively but divided by the fluid density ρ_f.

We note that the first three terms in 23 are very comparable to the terms seen in Eqs. (3.9) and (3.10) in [35]. We also note that it was proposed in [36] that the element lengths used in the second term (diffusive term) and third term (advective term) should be different, one being the diffusive element length and the other one being the advective element length. Nevertheless in the present work since the element length is evaluated and stored just at the beginning of the calculations it cannot be function of the velocity field. Furthermore, we note that as a way to address the issues related to including or not including the dynamic term in the stabilization, "element-vector-based" stabilization parameters were introduced in [37] and successfully tested in [10].

Table 1 Matrices and vectors of the semi discrete form of Eqs. 25

Matrix term		Continuum term
$\tilde{\mathbf{M}}_{ij}$		$\sum_j \int_\Omega N_i N_j d\Omega$
$\tilde{\mathbf{K}}_{ij}$	$\tilde{\mathbf{K}}^C_{ij}(\mathbf{u}_{gf})$	$\int_\Omega N_i \left(\overline{\mathbf{u}}_{fg} \cdot \nabla N_j\right) d\Omega$
	$\tilde{\mathbf{K}}^\mu_{fij}$	$\int_\Omega \nu_{fi} \nabla N_i \cdot \nabla N_j d\Omega$
	$\tilde{\mathbf{K}}^D_{ij}(\mathbf{u}_{gf})$	$\sum_j \int_\Omega N_i \mathbf{u}_{fg} N_j d\Omega$
$\tilde{\nabla}_{ij}$		$\int_\Omega n_i N_i \nabla N_j d\Omega$
$\tilde{\mathbf{D}}_{ij}$		$\int_\Omega N_i \nabla N_j^T d\Omega$
$\tilde{\mathbf{F}}_{fi}$		$\int_\Omega n_i N_i d\Omega$

Table 2 Stabilization matrices and vectors of system 25

Matrix term	Continuum term
$\mathbf{S}^u_{ij}$	$\int_\Omega \tau_i (\overline{\mathbf{u}}_{fg} \cdot \nabla N_i)(\overline{\mathbf{u}}_{fg} \cdot \nabla N_j + E_2 \|\mathbf{u_{fg}}\| N_j) d\Omega$
$\mathbf{S}^\pi_{ij}$	$\int_\Omega \tau_i N_i (\overline{\mathbf{u}}_{fg} \cdot \nabla N_j + E_2 \|\mathbf{u_{fg}}\| N_j) d\Omega$
$\mathbf{S}^p_{ij}$	$\int_\Omega \tau_i \nabla N_i \cdot \nabla N_j d\Omega$
$\mathbf{S}^\xi_{ij}$	$\int_\Omega \tau_i N_i \nabla N_j d\Omega$

3.1.3 Discretization procedure

System 20 can be rewritten in a semi discrete form as

$$\tilde{\mathbf{M}} \partial_t \mathbf{u}_f + \tilde{\mathbf{K}}^C \left(\mathbf{u}_{gf}\right) \mathbf{u}_f + \nabla \mathbf{p}_f + \tilde{\mathbf{K}}^\mu_f \mathbf{u}_f + \tilde{\mathbf{K}}^D \left(\mathbf{u}_{gf}\right) \mathbf{u}_f + \mathbf{S}^u \mathbf{u}_f - \mathbf{S}^\pi \boldsymbol{\pi} - \tilde{\mathbf{F}}_f = \mathbf{0}; \tag{24a}$$

$$\tilde{\mathbf{D}} \mathbf{u}_f + \mathbf{S}^p \mathbf{p}_f - \mathbf{S}^\xi \boldsymbol{\xi} = \mathbf{0}; \tag{24b}$$

$$\tilde{\mathbf{M}} \boldsymbol{\pi} - \tilde{\mathbf{K}}^C (\mathbf{u}_{gf}) \mathbf{u}_f = \mathbf{0}; \tag{24c}$$

$$\tilde{\mathbf{M}} \boldsymbol{\xi} - \tilde{\nabla} \mathbf{p}_f = \mathbf{0}; \tag{24d}$$

where $\mathbf{u}_f$ is the vector of nodal velocities and $\mathbf{p}_f$ the vector of nodal pressures. $\mathbf{u}_{gf}$ is the fluid velocity on the Gauss point. The operators take the form presented in Table 1 and the stabilization operators $\mathbf{S}^i$ are defined as shown in Table 2.

In order to simplify the problem, Eqs. 24c and 24d can be substituted in Eqs. 24a and 24b respectively, resulting

$$\tilde{\mathbf{M}}\partial_t \mathbf{u}_f + \tilde{\mathbf{K}}^C\left(\mathbf{u}_{g\,f}\right)\mathbf{u}_f + \nabla \mathbf{p}_f + \tilde{\mathbf{K}}^{\mu}_f \mathbf{u}_f + \tilde{\mathbf{K}}^D\left(\mathbf{u}_{g\,f}\right)\mathbf{u}_f + \mathbf{S}^u \mathbf{u}_f - \mathbf{S}^{\pi}\tilde{\mathbf{M}}^{-1}\tilde{\mathbf{K}}^C(\mathbf{u}_{g\,f})\mathbf{u}_f - \tilde{\mathbf{F}}_f = \mathbf{0}; \tag{25a}$$

$$\tilde{\mathbf{D}}\mathbf{u}_f + \mathbf{S}^p \mathbf{p}_f - \mathbf{S}^{\xi}\tilde{\mathbf{M}}^{-1}\tilde{\nabla}\mathbf{p}_f = 0; \tag{25b}$$

The residual of the momentum equations without the dynamic term is defined as

$$\begin{aligned}\tilde{\mathbf{r}}\left(\mathbf{u}_f, \mathbf{p}_f\right) := {} & \tilde{\mathbf{K}}^C\left(\mathbf{u}_{g\,f}\right)\mathbf{u}_f + \nabla \mathbf{p}_f + \tilde{\mathbf{K}}^{\mu}_f \mathbf{u}_f \\ & + \tilde{\mathbf{K}}^D\left(\mathbf{u}_{g\,f}\right)\mathbf{u}_f + \mathbf{S}^u \mathbf{u}_f \\ & - \mathbf{S}^{\pi}\tilde{\mathbf{M}}^{-1}\tilde{\mathbf{K}}^C(\mathbf{u}_{g\,f})\mathbf{u}_f - \tilde{\mathbf{F}}_f;\end{aligned} \tag{26}$$

3.1.4 *Fractional step solver using an explicit fourth order Runge Kutta time scheme*

The modified form of the Navier-Stokes equations is solved using a fractional step algorithm.

Pressure-splitting approaches of the fractional-step type are very convenient due to their high computational efficiency for flows at high Re. The fundamental idea is to solve the momentum equation keeping the pressure fixed and later correcting the pressure to guarantee the satisfaction of the divergence constraint. The fractional step approach is traditionally presented in an implicit context, typically using a first or second order backward differentiation formula (BDF1 or BDF2 algorithm respectively) for the time integration of the momentum equation. In practice it is typically observed that, in dealing with free-surface problems, even fully implicit schemes are limited to time steps for which the free surface moves approximately one element length per time step. Such heuristic constraint is equivalent in essence, to a restriction on the practical Courant Friedrichs Lewy (CFL) number approaching the unit value. This implies that explicit schemes will be competitive provided that $CFL \approx 1$ can be used and meshes of sufficiently good quality can be generated. This motivates the use of an explicit form of the fractional step scheme (see [30]) based on the use of a fourth order Runge Kutta (RK4) in dealing with the momentum equation. This choice has a lower computational cost per step than an explicit time integration technique since does not require solving of a system of equations and its implementation is highly parallelizable.

RK4 makes use of the solution at t^n to evaluate the solution at time t^{n+1} by calculating the residual of the equations at a certain number of intermediate steps.

In order to fully explain every stage of the integration scheme applied to the momentum equation let us use the definition of the stabilized residual obtained in Eq. 26.

The semi-discrete form of the momentum equations in terms of the residuals at the intermediate stages is then

$$\begin{aligned}\tilde{\mathbf{M}}\frac{\mathbf{u}_f^{n+1}-\mathbf{u}_f^n}{\Delta t} &= \frac{1}{6}\left[\tilde{\mathbf{r}}_{f\,1} + 2\,\tilde{\mathbf{r}}_{f\,2} + 2\,\tilde{\mathbf{r}}_{f\,3} + \tilde{\mathbf{r}}_{f\,4}\right]; \\ &= \frac{1}{6}\Big[\tilde{\mathbf{r}}_f(\mathbf{u}_f^n, \mathbf{p}_f^n) + 2\,\tilde{\mathbf{r}}_f(\mathbf{u}_f^{\theta 1}, \mathbf{p}_f^{\theta 1}) \\ &\quad + 2\;\tilde{\mathbf{r}}_f(\mathbf{u}_f^{\theta 2}, \mathbf{p}_f^{\theta 2}) + \tilde{\mathbf{r}}_f(\mathbf{u}_f^{\theta 3}, \mathbf{p}_f^{\theta 3})\Big];\end{aligned} \tag{27}$$

where $\tilde{\mathbf{r}}_f(\mathbf{u}_f^{\theta_i}, \mathbf{p}_f^{\theta_i})$ are the residuals of the momentum equations defined by Eq. 26 evaluated at θ_i intermediate stages.

To exactly evaluate the residual at each intermediate time step, the solution of the continuity equation is required. This would considerably reduce the efficiency, requiring a huge computational effort. In order to overcome this issue, according to [32], a linear variation of pressure is assumed in the time step. It should be remarked that this assumption leads the velocity field to be divergence free only at the end of the step.

Redefining Eq. 26 as

$$\tilde{\mathbf{r}}_f(\mathbf{u}_f, \mathbf{p}_f) = \tilde{\mathbf{r}}^u_f(\mathbf{u}_f) + \tilde{\mathbf{r}}^p_f(\mathbf{p}_f); \tag{28}$$

being $\tilde{\mathbf{r}}^u_f(\mathbf{u}_f)$ the part of the residual related to velocity and $\tilde{\mathbf{r}}^{\mathbf{p}}_f(\mathbf{p}_f)$ the part related to the pressure gradients. The residuals become

$$\begin{aligned}\tilde{\mathbf{r}}_{f\,1} &:= \tilde{\mathbf{r}}_f(\mathbf{u}_f^n, \mathbf{p}_f^n) = \tilde{\mathbf{r}}^u_f(\mathbf{u}_f^n) + \tilde{\nabla}\mathbf{p}_f^n; \\ \tilde{\mathbf{r}}_{f\,2} &:= \tilde{\mathbf{r}}_f(\mathbf{u}_f^{\theta 1}, \mathbf{p}_f^{\theta 1}) = \tilde{\mathbf{r}}^u_f(\mathbf{u}_f^{\theta 1}) + \frac{1}{2}\left(\tilde{\nabla}\mathbf{p}_f^n + \tilde{\nabla}\mathbf{p}_f^{n+1}\right); \\ \tilde{\mathbf{r}}_{f\,3} &:= \tilde{\mathbf{r}}_f(\mathbf{u}_f^{\theta 2}, \mathbf{p}_f^{\theta 2}) = \tilde{\mathbf{r}}^u_f(\mathbf{u}_f^{\theta 2}) + \frac{1}{2}\left(\tilde{\nabla}\mathbf{p}_f^n + \tilde{\nabla}\mathbf{p}_f^{n+1}\right); \\ \tilde{\mathbf{r}}_{f\,4} &:= \tilde{\mathbf{r}}_f(\mathbf{u}_f^{\theta 3}, \mathbf{p}_f^{\theta 3}) = \tilde{\mathbf{r}}^u_f(\mathbf{u}_f^{\theta 3}) + \tilde{\nabla}\mathbf{p}_f^{n+1}.\end{aligned} \tag{29}$$

And the global momentum equation 27 can be symbolically rewritten as

$$\begin{aligned}\tilde{\mathbf{M}}\frac{\mathbf{u}_f^{n+1}-\mathbf{u}_f^n}{\Delta t} &= \frac{1}{6}\Big[\tilde{\mathbf{r}}^u_f(\mathbf{u}_f^n) + 2\,\tilde{\mathbf{r}}^u_f(\mathbf{u}_f^{\theta 1}) \\ &\quad + 2\,\tilde{\mathbf{r}}^u_f(\mathbf{u}_f^{\theta 2}) + \tilde{\mathbf{r}}^u_f(\mathbf{u}_f^{\theta 3})\Big] \\ &\quad + \frac{1}{2}\left[\tilde{\nabla}\mathbf{p}_f^n + \tilde{\nabla}\mathbf{p}_f^{n+1}\right]\end{aligned} \tag{30}$$

In order to decouple the solution for the velocity and pressure, the traditional pressure splitting procedure is performed and the fractional step velocity $\tilde{\mathbf{u}}_f$ is inserted. This gives

$$\tilde{\mathbf{M}}\frac{\tilde{\mathbf{u}}_f-\mathbf{u}_f^n}{\Delta t}=\frac{1}{6}\left[\tilde{\mathbf{r}}_f^u(\mathbf{u}_f^n)+2\,\tilde{\mathbf{r}}_f^u(\tilde{\mathbf{u}}_f^{\theta 1})+2\,\tilde{\mathbf{r}}_f^u(\tilde{\mathbf{u}}_f^{\theta 2})+\tilde{\mathbf{r}}^u(\tilde{\mathbf{u}}_f^{\theta 3})\right]+\frac{1}{2}\tilde{\nabla}\mathbf{p}_f^n; \tag{31a}$$

$$\tilde{\mathbf{M}}\frac{\mathbf{u}_f^{n+1}-\tilde{\mathbf{u}}_f}{\Delta t}+\frac{1}{2}\tilde{\nabla}(\mathbf{p}_f^{n+1}-\mathbf{p}_f^n)=\mathbf{0}; \tag{31b}$$

$$\tilde{\mathbf{D}}\mathbf{u}_f^{n+1}+\mathbf{S}^p\mathbf{p}_f^{n+1}-\mathbf{S}^{\xi}\tilde{\mathbf{M}}^{-1}\tilde{\mathbf{G}}\mathbf{p}_f^{n+1}=0; \tag{31c}$$

where it has to be remarked that equation 31a only depends on the pressure at the previous time step and on the intermediate fractional step velocities, leading to a slightly different RK4 steps as explained later on.

From equation 31b

$$\mathbf{u}_f^{n+1}=\tilde{\mathbf{u}}_f-\frac{\Delta t}{2}\tilde{\mathbf{M}}^{-1}\tilde{\nabla}(\mathbf{p}_f^{n+1}-\mathbf{p}_f^n); \tag{32}$$

that substituted in equation 31c gives

$$\tilde{\mathbf{D}}\tilde{\mathbf{u}}_f-\frac{\Delta t}{2}\mathbf{D}\tilde{\mathbf{Q}}^{-1}_{M}\tilde{\nabla}(\mathbf{p}_f^{n+1}-\mathbf{p}_f^n)+\mathbf{S}^p\mathbf{p}_f^{n+1}-\mathbf{S}^{\xi}\tilde{\mathbf{M}}^{-1}\tilde{\mathbf{G}}\mathbf{p}_f^{n+1}=0. \tag{33}$$

Finally substituting the discrete Laplacian ($\tilde{\mathbf{D}}\tilde{\mathbf{M}}^{-1}\tilde{\nabla}$) by the continuous one ($\mathbf{L}$), the final system to be solved is:

$$\tilde{\mathbf{M}}\frac{\tilde{\mathbf{u}}_f-\mathbf{u}_f^n}{\Delta t}=\frac{1}{6}\left[\tilde{\mathbf{r}}_f^u(\tilde{\mathbf{u}}_f^n)+2\,\tilde{\mathbf{r}}_f^u(\tilde{\mathbf{u}}_f^{\theta 1})+2\,\tilde{\mathbf{r}}_f^u(\tilde{\mathbf{u}}_f^{\theta 2})+\tilde{\mathbf{r}}_f^u(\tilde{\mathbf{u}}_f^{\theta 3})\right]+\frac{1}{2}\tilde{\nabla}\mathbf{p}_f^n; \tag{34a}$$

$$\frac{\Delta t}{2}\mathbf{L}\left(\mathbf{p}_f^{n+1}-\mathbf{p}_f^n\right)=\tilde{\mathbf{D}}\tilde{\mathbf{u}}_f+\mathbf{S}^p\mathbf{p}_f^{n+1}-\mathbf{S}^{\xi}\tilde{\mathbf{M}}^{-1}\tilde{\mathbf{G}}\mathbf{p}_f^{n+1}; \tag{34b}$$

$$\mathbf{u}_f^{n+1}=\tilde{\mathbf{u}}_f-\frac{\Delta t}{2}\tilde{\mathbf{M}}^{-1}\tilde{\nabla}\left(\mathbf{p}_f^{n+1}-\mathbf{p}_f^n\right); \tag{34c}$$

where the residuals of Eq. 34a are evaluated according to the following steps

$$\tilde{\mathbf{r}}_f^u(\mathbf{u}_f^n); \tag{35a}$$

$$\tilde{\mathbf{u}}_f^{\theta 1}=\mathbf{u}_f^n+\tilde{\mathbf{M}}^{-1}\frac{\Delta t}{2}\left[\tilde{\mathbf{r}}_f^u(\mathbf{u}_f^n)+\tilde{\nabla}\mathbf{p}_f^n\right]; \tag{35b}$$

$$\tilde{\mathbf{r}}_f^u(\tilde{\mathbf{u}}_f^{\theta 1}); \tag{35c}$$

$$\tilde{\mathbf{u}}_f^{\theta 2}=\mathbf{u}_f^n+\tilde{\mathbf{M}}^{-1}\frac{\Delta t}{2}\left[\tilde{\mathbf{r}}_f^u(\tilde{\mathbf{u}}_f^{\theta 1})+\frac{1}{2}\tilde{\nabla}\mathbf{p}_f^n\right]; \tag{35d}$$

$$\tilde{\mathbf{r}}_f^u(\tilde{\mathbf{u}}_f^{\theta 2}) \tag{35e}$$

$$\tilde{\mathbf{u}}_f^{\theta 3}=\mathbf{u}_f^n+\tilde{\mathbf{M}}^{-1}\Delta t\left[\tilde{\mathbf{r}}_f^u(\tilde{\mathbf{u}}_f^{\theta 2})+\frac{1}{2}\tilde{\nabla}\mathbf{p}_f^n\right]; \tag{35f}$$

$$\tilde{\mathbf{r}}_f^u(\tilde{\mathbf{u}}_f^{\theta 3}); \tag{35g}$$

3.1.5 Level set

Since the technique we propose is based on the use of a fixed-grid approach, the solution method has to be completed by the choice of a tracking method for the free surface and by the choice of an approach to apply the boundary conditions needed on the free surface.

The *level set method* was conceived as a methodology to follow moving interfaces. The interface is implicitly defined as the zero-valued iso-surface of a given smooth function [26]. As often done, the level set function is defined as a signed distance function.

The developed technique consists of three parts:

- An *extrapolation function*: it defines the values of velocity, pressure and gradient of pressure on the nodes in the non-fluid area close to the free surface.
- A tool for the calculation of the *nodal distance* in the whole control domain once the new free surface has been defined;
- A way to choose the pressure to be applied on the outer nodes so that the pressure is approximately zero on the free surface.

A detailed description of the procedure developed by the authors can be found in [30].

3.2 Structural numerical model

The balance equation governing the structural problem detailed in Eqs. 14 and 15 are written here in a more compact form and considering the Lagrangian form of the problem.

Calling $\Omega_s \subset \mathbb{R}^d$ (where d is the space dimension) the structural domain in a time interval $(0, T)$, the modified Navier-Stokes equations are

$$\rho_s\partial_t\mathbf{u}_s+\nabla p_s'-2\nabla\cdot\tilde{\mu}\nabla^s\mathbf{u}_s-\rho_s\bar{\mathbf{b}}=\mathbf{0}\ \text{in}\ \Omega_s,\ t\in(0,T),$$
$$\nabla\cdot\mathbf{u}_s=0\ \text{in}\ \Omega_s,\ t\in(0,T), \tag{36}$$

where $-\rho_s\bar{\mathbf{b}}_s=-\rho_s\mathbf{b}_s+(1-n)\nabla p_f-\mathbf{D}$ according to what is explained in Remark 1. The problem is fully defined with the boundary and initial conditions 15.

Using the Galerkin formulation the weak form of the structural problem becomes

$$\int_\Omega \mathbf{w}_s \rho_s \partial_t \mathbf{u}_s d\Omega + \int_\Omega \mathbf{w}_s \nabla p'_s d\Omega$$
$$- \int_\Omega \mathbf{w}_s \nabla \cdot 2\tilde{\mu} \nabla^s \mathbf{u}_s d\Omega - \int_\Omega \mathbf{w}_s \rho_s \bar{\mathbf{b}}_s d\Omega = \mathbf{0} \quad \forall \mathbf{w}_s \in \mathcal{V},$$
$$\int_\Omega q_s \nabla \cdot \mathbf{u}_s = 0 \quad \forall q_s \in \mathcal{Q}, \tag{37}$$

where, for a fixed $t \in (0, T)$, $\mathbf{u}_s$ is assumed to belong to the velocity space $\mathcal{V} \in [\mathbf{H}^1(\Omega)]^d$ of vector functions whose components and their 1^{st} derivatives are square-integrable, and p'_s belongs to the pressure space $\mathcal{Q} \in \mathbf{L}_2$ of square-integrable functions. $\mathbf{w}_s$ and q_s are velocity and pressure weight functions belonging to velocity and pressure space respectively.

Performing the integration by part of the pressure and the viscous terms, gives

$$\int_\Omega \mathbf{w}_s \rho_s \partial_t \mathbf{u}_s d\Omega - \int_\Omega p'_s \nabla \cdot \mathbf{w}_s d\Omega$$
$$+ 2\int_\Omega \nabla \mathbf{w}_s : \tilde{\mu} \nabla^s \mathbf{u}_s d\Omega - \int_\Omega \mathbf{w}_s \rho_s \mathbf{b}_s d\Omega$$
$$- \int_{\partial\Omega_N} \mathbf{w}_s \cdot \mathbf{h} d\Gamma = \mathbf{0} \quad \forall \mathbf{w}_s \in \mathcal{V},$$
$$\int_\Omega q_s \nabla \cdot \mathbf{u}_s d\Omega = 0 \quad \forall q_s \in \mathcal{Q}, \tag{38}$$

Let $\mathcal{V}_h$ be a finite element space to approximate $\mathcal{V}$, and $\mathcal{Q}_h$ a finite element approximation to $\mathcal{Q}$. The problem is now finding $\mathbf{u}_{s\,h} \in \mathcal{V}_h$ and $p_{s\,h} \in \mathcal{Q}_h$ such that

$$\int_\Omega \mathbf{w}_{s\,h} \rho_s \partial_t \mathbf{u}_{s\,h} d\Omega - \int_\Omega p'_{s\,h} \nabla \cdot \mathbf{w}_{s\,h} d\Omega$$
$$+ 2\int_\Omega \nabla \mathbf{w}_{s\,h} : \tilde{\mu} \nabla^s \mathbf{u}_{s\,h} d\Omega - \int_\Omega \mathbf{w}_{s\,h} \rho_s \bar{\mathbf{b}}_s d\Omega$$
$$- \int_{\partial\Omega_N} \mathbf{w}_{s\,h} \cdot \mathbf{t}_{s\,h} d\Gamma = \mathbf{0} \quad \forall \mathbf{w}_{s\,h} \in \mathcal{V}_h,$$
$$\int_\Omega q_{s\,h} \nabla \cdot \mathbf{u}_{s\,h} d\Omega = 0 \quad \forall q_{s\,h} \in \mathcal{Q}_h. \tag{39}$$

3.2.1 Stabilized formulation

The choice of adopting equal order linear elements (P1/P1) for the velocity and pressure, despite its simplicity, entails the necessity of using a stabilization technique. An ASGS stabilization technique is employed for that purpose.

Table 3 Elemental stabilization terms in ASGS for the non-Newtonian element

Momentum equation	
$\mathcal{P}_s^m(\mathbf{w}_{s\,h})$	$\nabla q_{s\,h}$
$\tau_{s\,1}$	$\left(\frac{\alpha}{\Delta t} + \frac{4\tilde{\mu}}{h^2 \rho_s}\right)^{-1}$
$\mathcal{R}_s^m(\mathbf{u}_{s\,h})$	$\partial_t \mathbf{u}_{s\,h} - \nabla \cdot \frac{\tilde{\mu}}{\rho_s} \nabla^s \mathbf{u}_{s\,h} + \nabla p'_{s\,h} - \bar{\mathbf{b}}_s$
Continuity equation	
$\mathcal{P}_s^c(\mathbf{w}_{s\,h})$	$\nabla \cdot \mathbf{w}_{s\,h}$
$\tau_{s\,2}$	$\frac{\tilde{\mu}}{\rho_s}$
$\mathcal{R}_s^c(\mathbf{u}_{s\,h})$	$\nabla \cdot \mathbf{u}_{s\,h}$

The stabilized form of the balance equations becomes

$$\int_\Omega \mathbf{w}_{s\,h} \rho_s \partial_t \mathbf{u}_{s\,h} d\Omega - \int_\Omega p'_{s\,h} \nabla \cdot \mathbf{w}_{s\,h} d\Omega$$
$$+ 2\int_\Omega \nabla^s \mathbf{w}_{s\,h} : \tilde{\mu} \nabla \mathbf{u}_{s\,h} d\Omega - \int_\Omega \mathbf{w}_{s\,h} \rho_s \bar{\mathbf{b}}_s d\Omega$$
$$- \int_{\partial\Omega_N} \mathbf{w}_{s\,h} \mathbf{t}_{s\,h} d\Gamma + \sum_{el} \int_{\Omega^{el}} \tau_{s\,1} \mathcal{P}_s^m \cdot \mathcal{R}_s^m d\Omega = \mathbf{0} \tag{40}$$
$$\forall \mathbf{w}_{s\,h} \in \mathcal{V}_h,$$
$$\int_\Omega q_{s\,h} \nabla \cdot \mathbf{u}_{s\,h} d\Omega + \sum_{el} \int_{\Omega^{el}} \tau_{s\,2} \mathcal{P}_s^c \cdot \mathcal{R}_s^c d\Omega = 0$$
$$\forall q_{s\,h} \in \mathcal{Q}_h,$$

where $\mathcal{P}_s^m$, $\mathcal{R}_s^m$, $\mathcal{P}_s^c$ and $\mathcal{R}_s^c$ are defined in Table 3.

In a Lagrangian framework the convective term is not present. Therefore only pressure stabilization is required.

3.2.2 Discretization procedure

The matrix form of the stabilized system of Eqs. 40 can be written as:

$$\begin{bmatrix} \mathbf{M} & \mathbf{0} \\ \mathbf{0} & \mathbf{0} \end{bmatrix} \cdot \begin{bmatrix} \dot{\mathbf{u}}_s \\ \dot{\mathbf{p}}_s \end{bmatrix} + \begin{bmatrix} (\mathbf{K} + \mathbf{S}^c) & \mathbf{G} \\ (\mathbf{D} + \mathbf{S}_{qu}) & \mathbf{S}_{pq} \end{bmatrix} \cdot \begin{bmatrix} \mathbf{u}_s \\ \mathbf{p}_s \end{bmatrix} = \begin{bmatrix} \mathbf{F}_s \\ \mathbf{S}_q^f \end{bmatrix} \tag{41}$$

where the operators are explicitly written in Table 4 and the stabilization operators can be found in Table 5.

3.2.3 Bossak time integration scheme

A Bossak time integration scheme is used to advance in time the momentum equations.

Equations 41 can be written in compact form as

$$\overline{\mathbf{M}} \dot{v}_s + \mathbf{f}_{s\,int}(\mathbf{v}_s(t), t) = \mathbf{f}_{s\,ext}(t). \tag{42}$$

Table 4 Matrices and vectors of system 41 without stabilization terms

Matrix term	Continuum term
$\mathbf{M}\dot{\mathbf{u}}_s$	$\sum_{el}\int_{\Omega_{el}} \mathbf{w}_{s\,h}\rho_s\partial_t\mathbf{u}_{s\,h}d\Omega$
$\mathbf{K}\mathbf{u}_s$	$2\sum_{el}\int_{\Omega_{el}} \mathbf{w}_{s\,h}\nabla\mathbf{w}_{s\,h} : \tilde{\mu}\nabla\mathbf{u}_{s\,h}d\Omega$
$\mathbf{G}\mathbf{p}'_s$	$-\sum_{el}\int_{\Omega_{el}} p'_{s\,h}\nabla\cdot\mathbf{w}_{s\,h}d\Omega$
$\mathbf{D}\mathbf{u}_s$	$\sum_{el}\int_{\Omega_{el}} q_{s\,h}\nabla\cdot\mathbf{u}_{s\,h}d\Omega$
$\mathbf{F}_s$	$\sum_{el}\int_{\Omega_{el}} \mathbf{w}_{s\,h}\rho_s\bar{\mathbf{b}}_s d\Omega$
$\mathbf{h}_s$	$\mathbf{0}$

Table 5 Stabilization matrices and vectors of system 41

Matricial term	Continuum term
Momentum equation	
$\mathbf{S}_{qu}\mathbf{u}_s$	$-\sum_{el}\int_{\Omega_{el}} \tau_1\nabla q_{s\,h}\nabla\cdot\frac{\tilde{\mu}}{\rho_s}\nabla^s\mathbf{u}_{s\,h}d\Omega$
$\mathbf{S}_{pq}\mathbf{p}'_s$	$\sum_{el}\int_{\Omega_{el}} \tau_{s1}\nabla q_{s\,h}\nabla p_{s\,h}d\Omega$
$\mathbf{S}_q^f$	$-\sum_{el}\int_{\Omega_{el}} \tau_{s1}\nabla q_{s\,h}\bar{\mathbf{b}}_{s\,h}d\Omega$
Continuity equation	
$\mathbf{S}^c\mathbf{u}_s$	$\sum_{el}\int_{\Omega_{el}} \tau_{s2}\nabla\cdot\mathbf{w}_{s\,h}\nabla\cdot\mathbf{u}_{s\,h}d\Omega$

The resulting residual of the momentum equations linearized in time is

$$\mathbf{r}_s(\mathbf{v}_s^{n+1-\alpha_B}) = -\overline{\mathbf{M}}\left(\frac{1-\alpha_B}{\gamma\Delta t}\mathbf{v}_s^{n+1}\right) - \mathbf{f}_{s\,int}^{n+1} + \mathbf{f}_{s\,ext}^{n+1} - \overline{\mathbf{M}}\left[\frac{1-\alpha_B}{\gamma\Delta t}\mathbf{v}_s^n + \frac{(1-\alpha_B)^2}{\gamma}\mathbf{P}_{\mathbf{s}}^n - \alpha_B\mathbf{P}_{\mathbf{s}}^n\right], \tag{43}$$

where $\mathbf{v}_s^T = [\mathbf{u}_s,\ \mathbf{p}'_s]$ and $\mathbf{P}_s^T = [\mathbf{R}_s,\ \mathbf{P}'_{\mathbf{s}}]$ are the vectors of unknowns and

$$\alpha_B \in \left[-\frac{1}{3}, 0\right], \qquad \delta = \frac{1-2\alpha_B}{2}, \qquad \beta = \frac{(1-\alpha_B)^2}{4}; \tag{44}$$

The famous α-method presented by Hilber Hughes and Taylor in 1977was proven to be more accurate than Bossak scheme when the numerical dissipation is maximal. However in this work the Bossak scheme was chosen because it presents some implementation advantages for non-linear problems as explained in [1].

3.2.4 Predictor multi corrector residual based strategy

The solution of the non linear problem is achieved using a residual based approach. A quasi Newton method allows the linearization of the non linear terms.

The final system to be solved, calling k the current iteration and $n+1$ the following time step is

$$\underbrace{-\frac{\partial\mathbf{r}_s(\mathbf{v}_s^{n+1,k})}{\partial\mathbf{v}_s^{n+1}}}_{LHS}\Delta\mathbf{v}_s^k = \underbrace{\mathbf{r}(\mathbf{v}_s^{n+1,k})}_{RHS}; \tag{45}$$

In Eq. 45 $\Delta\mathbf{v}^k := \mathbf{v}^{n+1,k+1} - \mathbf{v}^{n+1,k}$ and

$$\frac{\partial\mathbf{r}_s(\mathbf{v}_s^{n+1,k})}{\partial\mathbf{v}_s^{n+1}} = -\frac{\overline{M}}{\delta\Delta t} - \frac{\partial\mathbf{f}_{s\,int}^{n+1,k}}{\partial\mathbf{v}_s^{n+1}}; \tag{46}$$

3.2.5 The particle finite element method (PFEM)

The PFEM is a numerical method that uses a Finite Element mesh to discretize the physical domain and to integrate the differential governing equations [13]. The domain is modeled using an Updated Lagrangian Formulation. All the variables are assumed to be known in the current configuration at time t and they are brought to the next (or updated) configuration at time $t+dt$. The finite element method (FEM) is used to solve the continuum equations in a mesh built up from the underlying nodes (the particles). This is useful to model the separation of solid particles from the bed surface and to follow their subsequent motion as individual particles with a known density, an initial acceleration and a velocity subjected to gravity forces [25].

It is important to remark that in PFEM each particle is treated as a material point characterized by the density of the solid domain to which it belongs to. The global mass is obtained by integrating density at the different material points over the domain. The quality of the numerical solution depends on the discretization chosen as in the standard FEM. Adaptive mesh refinement techniques can be used to improve the solution in zones where large gradients of the fluid or the structure variables occur.

Since its first development especially focused on the simulation of free surface flows and breaking waves [13], PFEM has been successfully used in a wide range of fields. Just to mention some of them, it is used in FSI and coupled problems [22,24,31], multi-fluid problems [17], contact problems and geotechnical simulations [4,23] and fire engineering [16]. Moreover PFEM has also been successfully used in the implementation of Bingham plastics model for the simulation of landslides [8].

The basic ingredients of PFEM can be summarized in:

- An **Updated Lagrangian** kinematical description of motion;
- A fast **remeshing** algorithm;
- A boundary recognition method (**alpha-shape**);
- **FEM** for the solution of the governing equations;

3.3 Coupling

An explicit staggered coupling is used in the present work.

This is acceptable considering that:

- The adoption of a semi-explicit scheme for the fluid problem leads to the need of using time steps much smaller than for the fully implicit structural problem, to ensure stability. An implicit coupling would require adopting the smaller time step, i.e. the one the fluid solver, for both models, leading to an extremely expensive procedure;
- The coupling between the two models is weaker in one of the two directions. For the solution of the fluid problem, in fact, only the porosity distribution is needed to be transfered by the structural model. In other words, the shape of the rockfill slope or, more generally, the one of the granular material has to be transfered to the fixed fluid mesh. On the contrary the other way coupling, the fluid pressure and velocity are essential to correctly define the external forces acting on the rockfill material.

In summary the structural Lagrangian model is mapped on the Eulerian fixed mesh domain where, at the beginning of the simulation, the only available information is the inflow discharge and the control domain. The idea is that the fluid analysis step is evaluated once the distribution of porosity is mapped from the structural domain. The solution of the fluid problem is then mapped on the Lagrangian structural mesh. It is necessary to know the fluid pressure and the Darcy forces in order to evaluate correctly the external force term of the momentum equation in 36. Once this is done, the structural response can be calculated. Therefore, the granular domain deforms accordingly to the obtained velocity and pressure fields. This new deformed granular domain is finally mapped onto the Eulerian mesh in order to solve for the subsequent time step.

An element transfer method (EMT) is implemented for the mapping of the variable between the Eulerian fixed and the PFEM moving meshes. The searching algorithm developed uses a kd-tree data structure.

The main steps of the entire simulation process are shown in Fig. 2 and the flow chart of the algorithm are schematically summarized in the box below:

Coupling algorithm

Assuming known the solution of the coupled problem at time step t^n.

1. **Map** the configuration of the rockfill material in terms of POROSITY distribution on the Eulerian fluid domain;
2. **SOLVE** the water free surface flow problem calculating the VELOCITY and PRESSURE fields in an EULERIAN fixed mesh;
3. **Map** the FLUID VELOCITY and PRESSURE fields on the Lagrangian structural mesh;
4. **Map** the non linear DARCY TERM on the Lagrangian structural mesh;
5. **CALCULATE** the structural response in a Lagrangian mesh, using PFEM;
6. Go back to step 1.

4 Numerical examples. Application to the failure of rockfill dams

In the present section the coupled model is validated through a comparison with the experimental results on scale models of rockfill dams in different seepage conditions, carried out by the Universidad Politécnica de Madrid (UPM) (Fig. 3), during the E-DAMS project (project of the National Plan R+D of the Spanish Ministry of Science and Innovation I+D BIA2010-21350-C03-00-2010-1013-).

Each experiment studies a scale model dam under a series of incremental "steps of inflow discharge". After each increment, the incoming discharge is maintained constant until reaching the steady state (Fig. 4). When a breach appears in the downstream slope, its stabilization is achieved before measuring its advance.

Pressure at the bottom of the flumes is evaluated by a sensors network. The deformation of the dam is analyzed through the evolution of the so called length of failure. It is, by definition, the horizontal projection of the distance between the initial undeformed downstream toe and the highest point of the failed area. The tracking of the failure line is performed using a *close-object-photogrammetry-technique*. It consists of taking a series of photos with a very short time interval until the end of the simulation. Through the post process of these data, the creation of a digital model of the deformed dam is possible and the dynamic evolution of the breach is followed with high precision.

In what follows an homogeneous dam is reproduced. No impermeabilization is present. The characteristics of the material used in the experiment are summarized in Table 6. The height of the scale model is 1 m, its width 2.46 m. The upstream and downstream slopes are both $1.5H{:}1V$ and the crest is 20 cm.

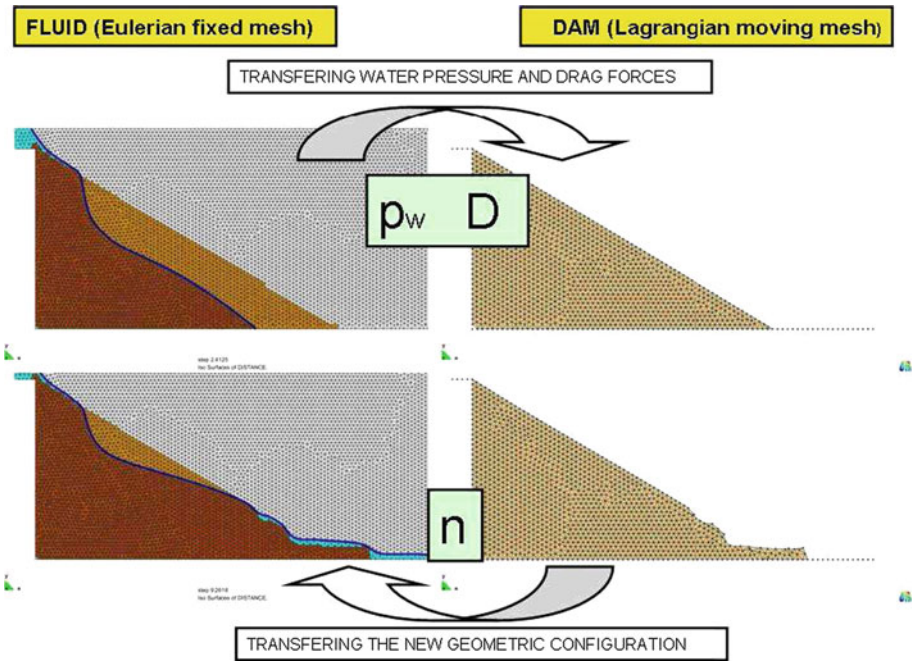

Fig. 2 Graphical summary of the whole process

Fig. 3 Experimental setting of the UPM laboratories

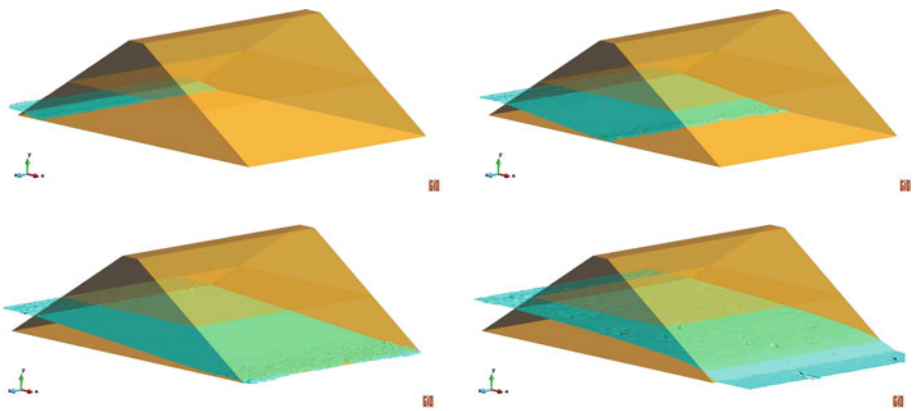

Fig. 4 Evolution of the seepage in the transient regime for a given inflow condition

Table 6 Properties of rockfill material

Porosity	n	0.4052
Average diameter	D_{50}	35.04 mm
Dry density	ρ_s	1490 kg/m^3
Saturated density	ρ_{sat}	1910 kg/m^3
Apparent specific weight	W	2500 kg/m^3
Pore index	P_i	0.68
Internal friction angle range	ϕ	[37°−42.5°]

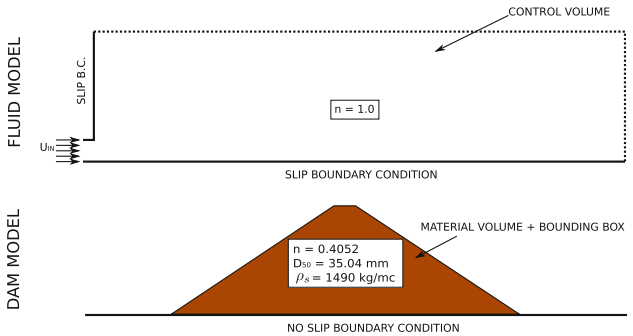

Fig. 5 Fluid and dam qualitative initial models and boundary conditions for the coupled analysis. *Upper image* the fluid Eulerian module. *Lower image* the structural PFEM one

In Fig. 5 a schematic view of the fluid and structure boundary conditions is shown. The mesh used for the fluid and the structural model is composed of 16 347 and 3 400 linear triangular elements respectively.

Four different incremental inflow discharges are considered to verify the capability of simulating the increment of rockfill failure of the presented approach. $Q_1 = 25.46\,\text{l/s}$ is the first inflow discharge, experimentally no deformation of the downstream slope was observed, $Q_2 = 51.75\,\text{l/s}$, $Q_3 = 69.07\,\text{l/s}$ and $Q_4 = 90.68\,\text{l/s}$. When the stationary regime for every boundary condition is achieved, the pressure head distribution and the advance of failure B is measured.

In the present work it was assumed that a particle is to be considered "moved" if its total numerical displacement is higher than the average dimension of the granular material (35 mm). This criterion was used in all the models analyzed in order to allow a comparative analysis.

Figure 6 show on the lower part the digital model obtained during the experiments, derived by the photogrammetric analysis, and on the upper part the contour fill of the displacements >35 mm. B_0 is the horizontal projection of the original slope of the downstream shoulder, whereas B in the upper and lower images indicates the numerical and experimental length of failure respectively. A summary of the values and the relative errors in the three cases analyzed is summarized in Table 7. A very good agreement is observed

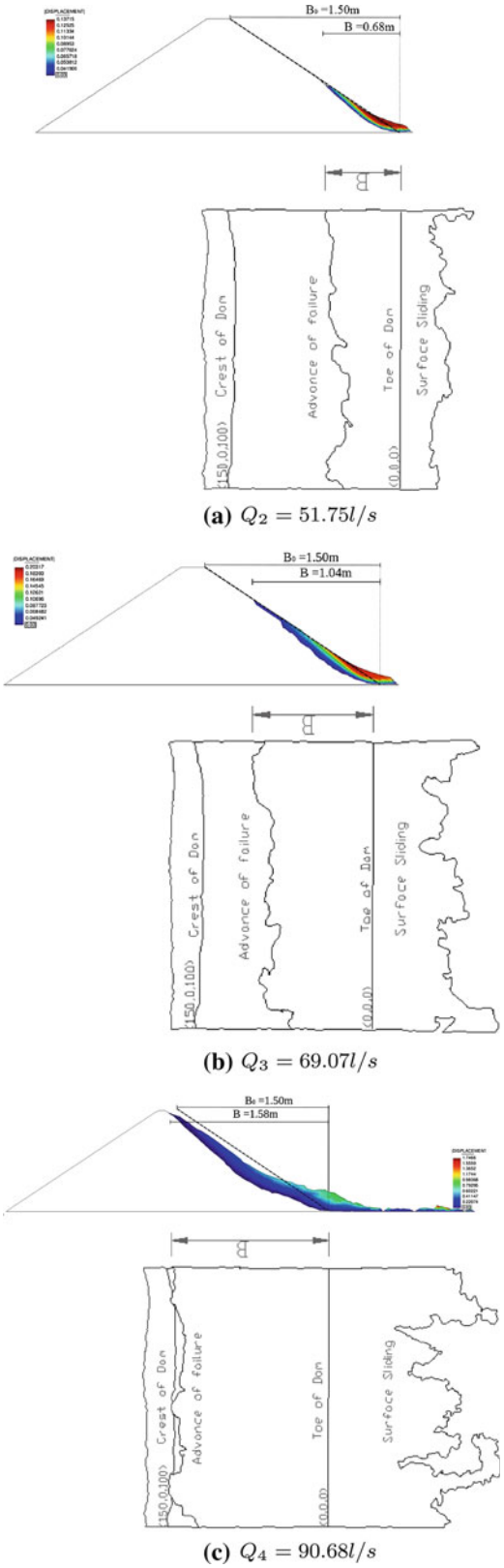

Fig. 6 Comparison between experimental and numerical lengths of failure for different inflow discharges. *Upper image* contour fill of numerical displacement > 35 mm. *Lower* digital model of the deformed slope in the experiments (plant view of the downstream shoulder)

Table 7 Comparison between experimental (B_{exp}) and numerical (B_{num}) length of failure for different discharges

Q $[l/s]$	B_{exp}	B_{num}	Error
25.46	0.0	0.0	0 %
51.75	0.71	0.68	4.2 %
69.07	1.08	1.04	3.7 %
90.68	1.56	1.58	1.3 %

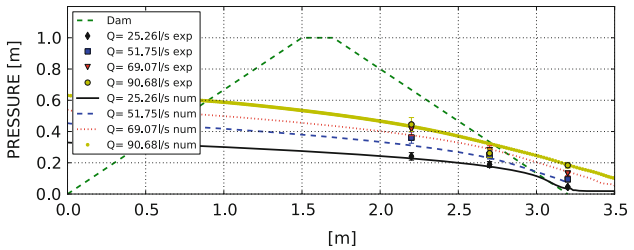

Fig. 7 Bottom pressure distribution at stationary regime for different discharges. Porosity $n = 0.4$, $D_{50} = 35$ mm. Numerical and experimental comparison

between experimental and numerical length of failure in the three cases.

The pressure head distributions obtained for the values of inflow discharges simulated, are summarized in Fig. 7. This shows that in the case with $Q = 90.68 l/s$, the pressure head presents a lower experimental value where the water exits the dam. The contraction of the flux can be induced by the absence of the rockfill that flowed away during the failure process in the experiments. This leads to the conclusion that the failed material in the numerical model settles faster than in the real case. Its accumulation over the original toe of the dam induces a higher value of pressure than in the experiment. This problem might be corrected by evaluating the superficial dragging induced by the water.

5 Conclusions

The main points of the present work can be summarized as follows:

1. A fluid code able to simulate the free surface flow over and throughout the rockfill have been developed. The classical Navier-Stokes equations have been modified to automatically account for a change in porosity values. The non linear seepage is evaluated using a quadratic form of the resistance law. Ergun's coefficients have been chosen. The possibility of including variable incoming discharges is included. A fixed mesh approach has been used and a level set technique has been implemented to track the evolution of the free surface both outside and inside the rockfill.
2. A code to simulate the behaviour of a granular non-cohesive material has been implemented. A non-Newtonian modified Bingham law is used. This approach gives the possibility of considering a pressure sensitive resistance criteria. This was obtained by inserting a Mohr Coulomb failure criteria in the Bingham relation. Since the rockfill is expected to undergo severe deformation during the failure process, a Lagrangian approach is preferred to a fixed mesh one. PFEM was the adopted technique.
3. A strategy to couple the models mentioned in points one and two has been developed. This tool includes an algorithm for the data mapping between non matching meshes, being the structural and the fluid models in two different kinematic frameworks (the Lagrangian and the Eulerian one).

Acknowledgments The research was supported by the E-DAM project of the National Plan R+D of the Spanish Ministry of Science and Innovation I+D BIA2010-21350-C03-00, by ERC Advanced Grant RealTime project AdG-2009325 and ERC Advance Grant SAFECON Project AdG-267521.

References

1. Adam D, Wood W (1983) Comparison of Hilber–Hughes–Taylor and Bossak α methods for the numerical integration of vibration equations. Int J Numer Methods Eng 19:765–771
2. Biot M (1941) General theory of three dimensional consolidation. J Appl Phys 12:155–164
3. de Boer R (2000) Theory of porous media. Springer, Berlin
4. Carbonell J, Oñate E, Suárez B (2008) Modeling of ground exavation with the particle finite element method (pfem). ASCE J Eng Mech 136:455–463
5. Codina R (2000) A nodal-based implementation of a stabilized finite element method for incompressible flow problems. Int J Numer Methods Fluids 33:737–766
6. Codina R (2000) Pressure stability in fractional step finite element methods for incompressible flows. J Comput Phys 170:112–140
7. Codina R, Soto O (2004) Approximation of the incompressible Navier-Stokes equations using orthogonal subscale stabilization and pressure segregation on anisotropic finite element meshes. Comput Methods Appl Mech Eng 193:1403–1419
8. Cremonesi M, Frangi A, Perego U (2011) A lagrangian finite element approach for the simulation of water-waves induced by landslides. Comput Struct 89:1086–1093
9. Dadvand P, Rossi R, Oñate E (2010) An object-oriented environment for developing finite element codes for multi-disciplinary applications. Arch Comput Methods Eng 17:253–297
10. Hsu MC, Bazilevs Y, Calo V, Tezduyar TE, Hughes T (2010) Improving stability of stabilized and multiscale formulations in flow simulations at small time steps. Comput Methods Appl Mech Eng 199:828–840
11. ICOLD (1995) Bulletin 99, dam failures statistical analysis. ICOLD, Paris
12. Larese A (2012) A coupled Eulerian–PFEM model for the simulation of overtopping in rockfill dams. PhD Thesis. Universitat Politècnica de Catalunya. UPC BarcelonaTech, Barcelona

13. Larese A, Rossi R, Oñate E, Idelsohn S (2008) Validation of the particle finite element method (PFEM) for simulation of free surface flows. Eng Comput 25:385–425
14. Lewis R, Schrefler B (1998) The finite element method for the static and dynamic deformation and consolidation of porous media. Wiley, New York
15. Lipscomb G, Denn M (1984) Flow of a bingham fluid in complex geometries. J Non Newtonian Fluid Mech 14:337–346
16. Marti J, Ryzhakov P, Idelsohn S, Oñate E (2012) Combined Eulerian–PFEM approach for analysis of polymers in fire situations. Int J Numer Methods Eng 81(2):135–268
17. Mier M, Idelsohn S, Oñate E (2010) Advances in the simulation of multi-fluid flows with the particle finite element method. Int J Numer Methods Fluids 67:1516–1539
18. Mossaiby F, Rossi R, Dadvand P, Idelsohn S (2011) OpenCL-based implementation of an unstructured edge-based finite element convection–diffusion solver on graphics hardware. Int J Numer Methods Eng 89(13):1635
19. Nield D, Bejan A (1992) Convection in porous media. Springer, New York
20. Nithiarasu P, Seetharamu K, Sundararajan T (1997) Natural convective heat transfer in a fluid saturated variable porosity medium. Int J Heat Mass Transf 40:3955–3967
21. Coussy O (1995) Mechanics of porous media. Wiley, New York
22. Oñate E, Celigueta M, Idelsohn S, Salazar F, Suarez B (2011) Possibilities of the particle finite element method for fluid–soil-structure interaction problems. J Comput Mech 48:307–318
23. Oñate E, Idelsohn S, Celigueta M, Rossi R (2008) Advances in the particle finite element method for the analysis of fluid multibody interaction and bed erosion in free surface flows. Comput Methods Appl Mech Eng 197:1777–1800
24. Oñate E, Idelsohn S, Celigueta M, Rossi R, Marti J, Carbonell J, Ryzakov P, Suárez B (2011) Advances in the particle finite element method (PFEM) for solving coupled problems in engineering. In: Oñate E, Owen R (eds) Particle-based methods, computational methods in applied sciences, vol 25. Springer, New York
25. Oñate E, Idelsohn S, Pin FD, Aubry R (2004) The particle finite element method an overview. Int J Comput Methods 1:267–307
26. Osher S, Fedkiw RP (2003) Level set methods and dynamic implicit surfaces. Springer, New York
27. Papanastasiou TC (1987) Flows of materials with yield. J Rheol 31:385–404
28. Quecedo M, Pastor M, Herreros M, Merodo JF (2004) Numerical modelling of the propagation of fast landslides using the finite element method. Int J Numer Methods Eng 59:755–794
29. Rojek J, Labra C, Su O, Oñate E (2012) Comparative study of different discrete element models and evaluation of equivalent micromechanical parameters. Int J Solids Struct 49:1497–1517
30. Rossi R, Larese A, Dadvand P, Oñate E (2012) An efficient edge-based level set finite element method for free surface flow problems. Int J Numer Methods Fluids. doi:10.1002/fld.3680
31. Ryzhakov P, Rossi R, Idelsohn S, Oñate E (2010) A monolithic lagrangian approach for fluid-structure interaction problems. Int J Comput Mech 46(6):883–899
32. Ryzhakov P, Rossi R, Oñate E (2011) An algorithm for the simulation of thermally coupled low speed flow problems. Int J Numer Methods Fluids 65:1217–1230
33. Soto O, Lohner R, Cebral J, Camelli F (2004) A stabilized edge-based implicit incompressible flow formulation. Comput Methods Appl Mech Eng 193:2139–2154
34. Taylor D (1948) Fundamentals of soil mechanics. Wiley, New York
35. Tezduyar T (1992) Stabilized finite element formulations for incompressible flow computations. Adv Appl Mech 28:1–44
36. Tezduyar T (2003) Computation of moving boundaries and interfaces and stabilization parameters. Int J Numer Methods Fluids 43:555–575
37. Tezduyar T, Osawa Y (2000) Finite element stabilization parameters computed for element matrices and vectors. Comput Methods Appl Mech Eng 190:411–430
38. Toledo M (1997) Presas De Escollera Sometidas a Sobrevertido. Estudio del Movimientos dal Agua a Través de la Escollera e de la Estabilidad Frente al Deslizamiento en Masa. PhD thesis: Universidad Politécnica de Madrid
39. Wellmann C, Wriggers P (2012) A two-scale model of granular materials. Comput Methods Appl Mech Eng 1:46–58
40. Zienkiewicz O, Chan A, Pastor M, Schrefler B, Shiomi T (1999) Computational geomechanics with special reference to earthquake engineering. Wiley, New York
41. Zienkiewicz O, Shiomi T (1984) Dynamic behaviour of saturated porous media: the generalised biot formulation and its numerical solution. Int J Numer Anal Methods Geomech 8:71–96